Halo suppression in full-field x-ray Zernike phase contrast microscopy

Ismo Vartiainen,[1,*] Rajmund Mokso,[1] Marco Stampanoni,[1,2] and Christian David[1]

[1]*Paul Scherrer Institut, CH-5232 Villigen PSI, Switzerland*

[2]*Institute for Biomedical Engineering, ETH and University Zürich, CH-8092, Zürich, Switzerland*

**Corresponding author: ismo.vartiainen@psi.ch*

Received November 21, 2013; revised February 7, 2014; accepted February 10, 2014;
posted February 11, 2014 (Doc. ID 201589); published March 12, 2014

Visible light Zernike phase contrast (ZPC) microscopy is a well established method for imaging weakly absorbing samples. The method is also used with hard x-ray photon energies for structural evaluation of material science and biological applications. However, the method suffers from artifacts that are inherent for the Zernike image formation. In this Letter, we investigate their origin and experimentally show how to suppress them in x-ray full-field ZPC microscopy based on diffractive x-ray optics. © 2014 Optical Society of America

OCIS codes: (340.6720) Synchrotron radiation; (340.7460) X-ray microscopy; (050.1970) Diffractive optics.
http://dx.doi.org/10.1364/OL.39.001601

X-ray microscopy has potential in imaging thick samples with high resolution due to the large penetration depth and the short wavelength of x rays. As a drawback, the absorption contrast is low, especially when imaging biological samples with hard x rays. Zernike phase contrast (ZPC) microscopy can be used to image samples that only cause a phase shift to the incident light [1,2]. The method is routinely applied for imaging various types of samples with visible light and x rays [3–5]. However, it suffers from artifacts that can be prominent in strongly phase-shifting samples. In particular, the image of sharp edges in the sample often shows echo-like features, referred to as halos (see, e.g., [6]). These halos can be so pronounced that it is difficult to distinguish them from the physical features of the sample, and thus they impede a quantitative analysis, e.g., in a tomographic reconstruction. Some methods have been proposed to reduce this problem, such as apodization of the phase shifter [7] or using an amplitude mask for illumination matched with the phase shifter [8]. These methods work fairly well in visible light microscopy, but are difficult to implement with x-ray photon energies. No detailed studies or experiments have been conducted with x-ray photon energies.

The key point in ZPC microscopy is that the diffracted light from the sample is spatially separated from the nondiffracted part in the back-focal plane (BFP) of the imaging lens. Therefore, the phase shift can be manipulated separately for either of these light paths. A quarter wave plate is generally used to transfer the phase difference of these two waves to amplitude modulation in the detector [2]. The amplitude variation in the ZPC image is directly related to phase shift induced by the sample. For a sharp separation of scattered and unscattered beams, the illumination angles need to be clearly defined. In visible light ZPC microscopes, the illumination is typically hollow cone, resulting in a ring of the unscattered radiation in the BFP. The hollow cone illumination in x-ray microscopes can be achieved by annular aperture with zone plates [9] or capillary condensers [10]. Zone plates with an annulus are inefficient due to the small effective aperture, whereas in the case of capillaries, illumination angles are not well controlled. Parallel illumination has also been applied in x-ray ZPC microscopy in order to reduce the halo effects [11]. However, this type of illumination compromises the achievable resolution and overall efficiency.

In this Letter, we demonstrate a method for halo suppression that is based on the setup shown in Fig. 1, minimizing the unwanted phase shift in the phase shifter. In addition, our setup makes the appearance of the residual halo smoother, making it well suited for quantitative analysis. Our setup is based on a beam shaper (BS) illumination and a Fresnel zone plate as an objective lens.

The experiment was carried out in the Swiss Light Source at the beamline for tomographic microscopy and coherent radiology experiments (TOMCAT) with 12 keV photons. For the illumination of the sample, we

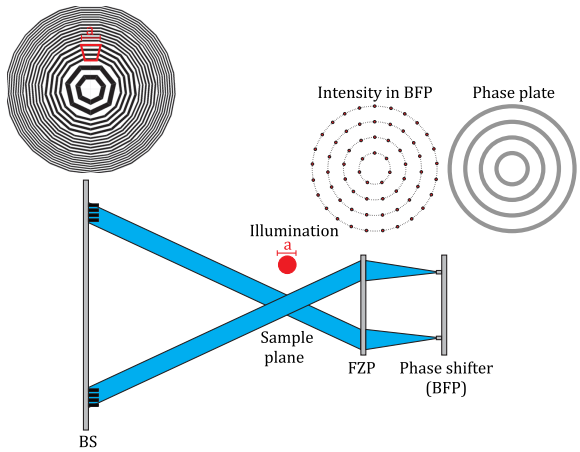

Fig. 1. Schematic of the setup. A beam shaper (BS) illuminates the sample from discrete angles that overlap in the sample plane, forming a flat top illumination in the sample plane. One of the individual gratings is outlined in red in the BS. Light paths from only two gratings in the BS are shown for simplicity. A zone plate focuses the nondiffracted plane waves to the phase shifter and projects a magnified image of the sample to the detector plane. A phase plate containing concentric rings is used to shift the phase of the zeroth order light by $\pi/2$. Central stop, order sorting aperture, and the detector are neglected from the schematic for brevity. The arrangement of these components is similar to [5].

follow an approach previously developed for amplitude contrast microscopy by Vogt *et al.* [12], and later developed for ZPC by Stampanoni *et al.* [5]. The beam-shaping condenser consists of binary gratings with constant period and angle arranged on a circular grid (Fig. 1). The period is determined by the zone plate equation; hence, in the sample plane, light coming from all of these gratings overlaps. This design has the following essential advantages: (i) a large area of the beam can be accepted by the BS, making the setup very photon efficient; (ii) it forms a uniform circular illumination; and (iii) the object is illuminated from a set of well-defined, discrete directions, and thus the unscattered radiation forms an array of sharp spots in the BFP of the imaging Fresnel zone plate, which lie on concentric circles around the optical axis (see Fig. 1). As will be discussed further, the latter point is important regarding the halo suppression. Similar conclusions have been made in visible light ZPC microscopy using discrete illumination by an amplitude mask [8].

The outermost zone width of the BS is 70 nm, the size of the individual gratings is 50 μm × 50 μm, and the BS's diameter is 1 mm [see Fig. 2(a)]. The source distance of the beam line is 19.5 m, leading to a focal distance of 665.6 mm, defined as the sample plane. A Fresnel zone plate with an outermost zone width of 70 nm and diameter 100 μm is used to focus the image of the sample to the detector. The zone plate is placed 68.23 mm downstream of the sample, and the detector, consisting of a scintillator screen, magnification optics, and a CCD sensor, is situated 9.5 m downstream of the zone plate. This leads to a magnification factor of 140. A phase shifter is placed in the BFP of the objective lens. The setup described leads to an effective pixel size of 57 nm × 57 nm in the object plane, taking into account the magnification provided by the x-ray microscope and the optical magnification after the scintillator in the detector. The BS and the Fresnel zone plate were fabricated on a thin Si_3N_4 membrane by electron beam lithography and Au electroplating [13]. The thickness of the structures was 1100 nm, leading to theoretical diffraction efficiency of up to 12% at 12 keV [14]. The Zernike phase shifter was fabricated on a thin silicon membrane by electron beam lithography and dry etching. The thickness of the silicon structures was 7.65 μm to achieve the required phase shift of $\pi/2$ at 12 keV photon energy [14].

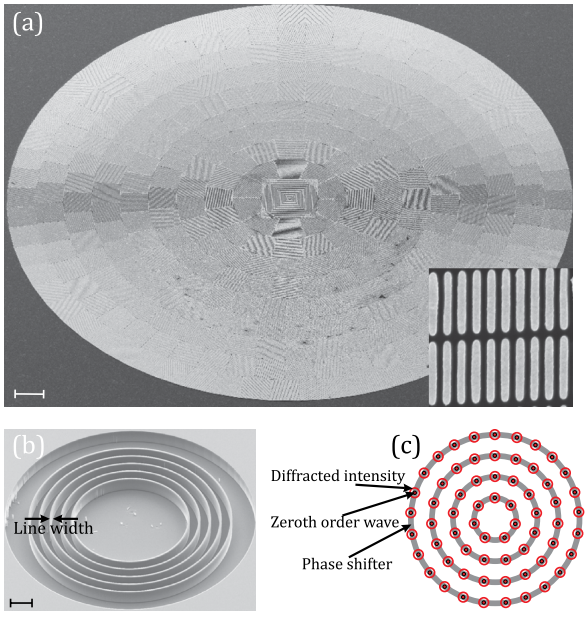

Fig. 2. Scanning electron microscopy images of the (a) BS and (b) phase rings. Inset in (a) shows the outermost zones of the BS. Image (c) illustrates the diffracted light from a circular object in the BFP of the objective lens. Scale bars in (a) and (b) are 50 and 10 μm, respectively.

For evaluation of the effect of the phase-shifter geometry, let us first consider a situation without a sample. The use of a BS described previously leads to an intensity distribution consisting of spots on a circular grid in the BFP of the objective lens. Every spot originates from one of the gratings in the BS (see Fig. 1). The phase shifter is used to phase shift only the unscattered light from the sample; thus, it should be designed according to this zeroth order intensity distribution. However, in our case, we used concentric rings [see Fig. 2(b)]. This phase-shifter design overlaps with the intensity distribution of the zeroth order wave [see Fig. 2(c)]. This design makes the setup much easier to align, as no rotational alignment is necessary. In addition, this design smears the halo partially, as no sharp cutoff frequency exists for the phase-shifted part due to the smooth transition provided by the ring structure.

The width of the rings in the phase shifter has a significant effect on the amplitude of the halo because ZPC depends on the spatial frequencies present in the object. In particular, the phase contrast goes to zero for objects that scatter to angles that are so small that all the scattered intensity goes through the phase shifter, and hence experience the same phase shift as the unscattered wave. This effect is called "shade-off" in the visible light microscopy. The scattering angles are defined by diffraction and thus, the larger features the object has, the smaller the separation of the nondiffracted and the diffracted parts of the light have in the BFP of the objective lens. For the reduction of halos, it is essential that this cutoff frequency be as low as possible, and that the transition is smooth in order to avoid sharp halos.

Let us next consider a sample that scatters part of the incident light away from the zeroth order beam. Figure 2(c) illustrates the diffraction in BFP caused by a circular object. Regardless of the spatial frequency of the sample, a small part of the diffracted light is always phase shifted by the ring structure, and the halo produced by the setup remains smooth. In order to minimize the unwanted phase shift of the scattered light, the line width (LW) of the phase shifter [see Fig. 2(b)] needs to be minimized. The minimum LW of the phase shifter is defined by the minimum spot size that the zone plate can produce. It should be noted that, in the case of incoherent illumination, this can be substantially larger than the diffraction-limited spot size.

Let us assume a monochromatic beam and a finite source distance of 19.5 m. Moreover, in the case of the TOMCAT beam line, the photon beam source size is 133 μm × 52 μm (FWHM) in the horizontal and vertical directions, respectively. The BS described previously

splits the incident beam into diverging beams with size of individual gratings and divergence the same as the incident beam. In our case, the grating width is 50 μm, which becomes the aperture size for deriving the minimal spot size of the nondiffracted beam in the BFP of the objective lens. We used a zone plate with a diameter of 100 μm as an objective lens, and hence the effective numerical aperture (NA) is half the NA of the zone plate. These numbers finally lead to minimal spot size of the nondiffracted beam in the BFP of the objective lens of 450 nm × 180 nm (FWHM) in horizontal and vertical directions, respectively, where the spot size is defined by a demagnified source.

During the experiment, we used a multilayer monochromator that has approximately 2% bandwidth, which further increases the spot size in the BFP of the objective lens by chromatic blurring [15]. In our case, the effect of chromatic blurring is on the order of 100 nm. By taking into account the effects of the source size, the effective NA of the zone plate, and the chromatic blurring, the minimal LW for the phase shifter using the current configuration is ≈500 nm. In order to test this effect, different LWs varying from 500 to 1500 nm were fabricated. Using smaller LWs is not feasible due to the fact that the tolerances in the alignment of the phase shifter in the beam direction become smaller with smaller LW. Here, it should be noted that the proposed design is generally very easy to align using a high-resolution x-ray camera placed just downstream of the BFP during the alignment phase. Due to the circular symmetry of the phase shifter and the zone plate, both can be overlapped to within less than a micrometer. The final alignment is then done by optimizing the contrast and the uniformity of contrast in the ZPC image.

Figure 3 shows the comparison of ZPC images of a Siemens star made of silicon that was used as a test sample by using different LWs of the phase shifter. The thickness of the silicon structures was 1000 nm, leading to a phase shift of $\pi/15$ at 12 keV. In addition

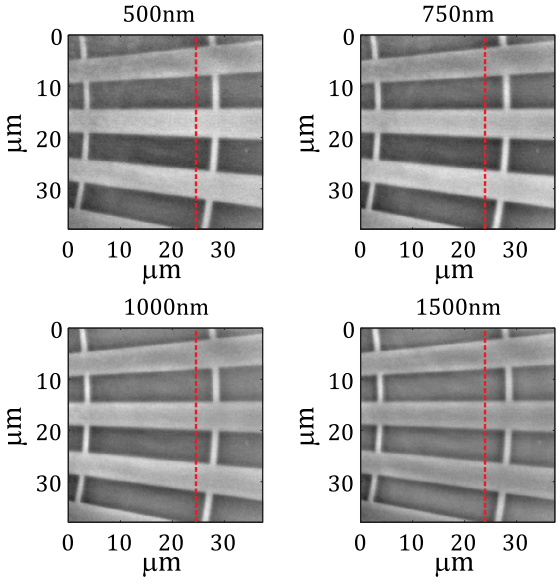

Fig. 3. ZPC images of the test sample using different LWs of the phase shifter.

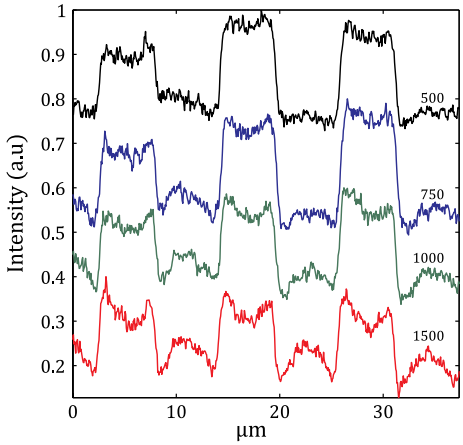

Fig. 4. Cross sections of the phase contrast images in Fig. 3 along the red lines. The cross sections for each LW are shifted vertically for better comparison.

to difference in halo, the contrast is also decreased in the case of larger phase shifter LW. This is due to the shade-off that is a result of phase shifting completely, and also the diffracted light from this specific spatial frequency of the sample. Therefore, the object is visible mainly because of the edge diffraction. From the line profiles shown in Fig. 4 it is clear that, by decreasing the LW in the phase shifter, the halos that occur as sharp features around the edges of the test object are decreased. From Figs. 3 and 4, it is evident that the halo is suppressed by using smaller LWs in the Zernike phase shifter.

Finally, we show the improvement in 3D image quality realized by the optimized phase rings in circular geometry as compared to the nonoptimized square geometry [5] of the TOMCAT x-ray microscope. In the case of the square geometry, the phase rings are replaced by the corresponding phase pillars of a diameter of 1 μm, as previously described in [5]. For the comparison, we did tomography on carbon fibers with diameter of 7 μm. Over a 180° rotation with the axis in the plane parallel to the length of the fibers, we acquired 361 equidistantly spaced angular projection images, each with 1.7 s exposure time and 57 nm pixel size, as described in detail in [16]. We used a Fourier-based tomographic reconstruction method [17] to obtain the 3D volumes. The carbon fibers are challenging test objects for x-ray phase contrast microscopy because they are almost pure phase samples with relatively large phase shift ($\pi/4$ at 12 keV), and have extremely well-defined edges. As explained previously, these features make the appearance of halos most prominent. Figure 5 presents the tomographic reconstruction of the carbon fibers for the optimized circular geometry and for the square BS case. The apparent sharp halo artifact in the images acquired in the square setup is significantly suppressed in the optimized configuration, allowing a more realistic interpretation of the resulting intensity profiles. Some artifacts remain in the region between the fibers in the direction of the largest phase shift ($>\pi$) introduced in the projection images at the angular direction parallel to alignment direction to the three fibers in the (horizontal) plane perpendicular to the tomographic rotation axis (vertical).

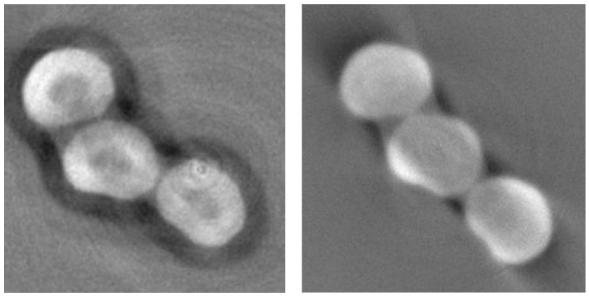

Fig. 5. Tomographic slices of three carbon fibers with 7 μm diameter acquired with the square BS configuration (left), and with the optimized phase rings in the circular geometry (right).

We have explained the origin of the main artifacts in the full-field x-ray ZPC microscopy. Moreover, we have shown how these artifacts can be minimized by proper design of the phase shifter. Experimental results clearly illustrate the effect of halo suppression with different test samples. In addition, we explain how this setup can be easily aligned compared to other designs used with x-ray microscopy. The use of diffractive optics enables precise control of light paths and can therefore be used to minimize the amount of unwanted phase shift that causes the halo. This is the largest difference compared to other illumination methods used in full-field x-ray microscopy, such as capillary condensers, where high uncertainty of the light paths exists.

The research leading to these results has received funding from the European Community's Seventh Framework Programme (FP7/2007-2013) under Grant Agreement No. 290605 (PSI-FELLOW/COFUND).

References

1. F. Zernike and Z. F. Techn, Z. Techn. Physik **16**, 454 (1935).
2. M. Born and E. Wolf, *Principles of Optics*, 7th ed. (Cambridge University, 1999), p. 472.
3. G. Schmahl, D. Rudolph, P. Guttmann, G. Schneider, J. Thieme, and B. Niemann, Rev. Sci. Instrum. **66**, 1282 (1995).
4. U. Neuhäusler, G. Schneider, W. Ludwig, M. A. Meyer, E. Zschech, and D. Hambach, J. Phys. D **36**, A79 (2003).
5. M. Stampanoni, R. Mokso, F. Marone, J. Vila-Comamala, S. Gorelick, P. Trtik, K. Jefimovs, and C. David, Phys. Rev. B **81**, 140105(R) (2010).
6. H. S. Youn and S.-W. Jung, J. Microsc. **223**, 53 (2006).
7. T. Otaki, Opt. Rev. **7**, 119 (2000).
8. P. Gao, B. Yao, I. Harder, N. Lindlein, and F. J. Torcal-Milla, Opt. Lett. **36**, 4305 (2011).
9. A. Tkachuk, F. Duewer, H. Cui, M. Feser, S. Wang, and W. Yun, Z. Kristallogr. **222**, 650 (2007).
10. P. Guttmann, X. Zeng, M. Feser, S. Heim, W. Yun, and G. Schneider, J. Phys. Conf. Ser. **186**, 012064 (2009).
11. J. Lim, S. Y. Park, J. Y. Huang, S. M. Han, and H.-T. Kim, Rev. Sci. Instrum. **84**, 013707 (2013).
12. U. Vogt, M. Lindblom, P. Charalambous, B. Kaulich, and T. Wilhein, Opt. Lett. **31**, 1465 (2006).
13. S. Gorelick, V. Guzenko, J. Vila-Comamala, and C. David, Nanotechnology **21**, 295303 (2010).
14. B. L. Henke, E. M. Gullikson, and J. C. Davis, At. Data Nucl. Data Tables **54**, 181 (1993).
15. Ch. Morawe, J.-P. Guigay, V. Mocella, and C. Ferrero, Opt. Express **16**, 16138 (2008).
16. R. Mokso, L. Quaroni, F. Marone, S. Irvine, J. Vila-Comamala, A. Blanke, and M. Stampanoni, J. Struct. Biol. **177**, 233 (2012).
17. F. Marone and M. Stampanoni, J. Synchrotron Radiat. **19**, 1029 (2012).